HHS Public Access

Author manuscript

J Invest Dermatol. Author manuscript; available in PMC 2015 January 01.

Published in final edited form as:

J Invest Dermatol. 2014 July ; 134(7): 1817–1827. doi:10.1038/jid.2014.94.

Loss of *Mpzl3* Function Causes Various Skin Abnormalities and Greatly Reduced Adipose Depots

Angel G. Leiva[1], **Anne L. Chen**[1], **Priyadharshini Devarajan**[2], **Zhibin Chen**[2], **Shadi Damanpour**[1], **Jessica A. Hall**[3], **Antonio C. Bianco**[3], **Jie Li**[1], **Evangelos V. Badiavas**[1,4], **Julia Zaias**[5], **Mariya Miteva**[1], **Paolo Romanelli**[1], **Keyvan Nouri**[1], and **Tongyu Cao Wikramanayake**[1,6]

[1]Department of Dermatology and Cutaneous Surgery, University of Miami Miller School of Medicine, Miami, Florida, U.S.A

[2]Department of Microbiology and Immunology, University of Miami Miller School of Medicine, Miami, Florida, U.S.A

[3]Division of Endocrinology, Department of Medicine, University of Miami Miller School of Medicine, Miami, Florida, U.S.A

[4]Interdisciplinary Stem Cell Institute, University of Miami Miller School of Medicine, Miami, Florida, U.S.A

[5]Comparative Pathology, University of Miami Miller School of Medicine, Miami, Florida, U.S.A

[6]Molecular Cell and Developmental Biology, Graduate Program in Biomedical Sciences, University of Miami Miller School of Medicine, Miami, Florida, U.S.A

Abstract

The rough coat (*rc*) spontaneous mutation causes sebaceous gland hypertrophy, hair loss and extracutaneous abnormalities including growth retardation. The *rc* mice have a missense mutation in the predicted immunoglobulin protein *Mpzl3*. In this study, we generated *Mpzl3* knockout mice to determine its functions in the skin. Homozygous *Mpzl3* knockout mice showed unkempt and greasy hair coat and hair loss soon after birth. Histological analysis revealed severe sebaceous gland hypertrophy and increased dermal thickness, but did not detect significant changes in the hair cycle. *Mpzl3* null mice frequently developed inflammatory skin lesions; however, the early onset skin abnormalities were not the results of immune defects. The abnormalities in the *Mpzl3* knockout mice resemble closely those observed in the *rc*/*rc* mice, as well as mice heterozygous for both the *rc* and *Mpzl3* knockout alleles, indicating that *rc* and *Mpzl3* are allelic. Using a *lacZ* reporter gene, we detected *Mpzl3* promoter activity in the companion layer and inner root sheath of the hair follicle, sebaceous gland, and epidermis. Loss of MPZL3 function also caused a

Correspondence: Tongyu Cao Wikramanayake, Ph.D., Department of Dermatology and Cutaneous Surgery, University of Miami Miller School of Medicine, 1600 NW 10th Avenue, RMSB 2023A, Miami, FL, 33136, U.S.A., Phone: (305)243-8878, Fax: (305)243-6191, tcao@med.miami.edu.

CONFLICT OF INTEREST

The authors declare no conflict of interest.

striking reduction in cutaneous and overall adipose tissue. These data reveal a complex role for *Mpzl3* in the control of skin development, hair growth and adipose cell functions.

Keywords

Mpzl3; sebaceous gland; hair follicle; alopecia; adipose

INTRODUCTION

The rough coat (*rc*) mutation is an autosomal recessive mutation that arose spontaneously in the C57BL/6J inbred mouse strain (Dickie, 1966; Eicher *et al.*, 1977). While named for their unkempt hair coat, the *rc*/*rc* mice also showed various other skin abnormalities including cyclic and progressive hair loss and sebaceous hypertrophy due to sebocyte hyperplasia (Cao *et al.*, 2007; Hayashi *et al.*, 2004; Ruvinsky *et al.*, 2002). Various extracutaneous abnormalities ((Hayashi *et al.*, 2004); unpublished observations) in the *rc*/*rc* mice suggest that the mutated gene is indispensible in multiple organ systems.

In a previous study, we reduced the *rc* mapping interval to 246kb, and identified a missense mutation in a novel gene we named Myelin Protein Zero-Like 3 (*Mpzl3*) (Cao *et al.*, 2007). *Mpzl3* encodes a predicted single-span transmembrane protein (Type I) with an immunoglobulin (Ig) v-type domain, and was so named because of its closest sequence homology to Myelin Protein Zero (*Mpz*) and Myelin Protein Zero-Like 2 (*Mpzl2*, also called EVA1) (Cao *et al.*, 2007). The biological functions of MPZL3 remained unclear (Racz *et al.*, 2009; Ramani *et al.*, 2012) until Czyzyk and colleagues showed in a recent study that *Mpzl3* played a major role in regulating metabolism and energy expenditure (Czyzyk *et al.*, 2013).

To better understand *Mpzl3* functions in the skin, we generated *Mpzl3* null mice, and analyzed skin abnormalities and *Mpzl3* promoter activity during the hair cycle. We also evaluated some extracutaneous abnormalities in the *Mpzl3* null mice and *rc/rc* mice.

RESULTS

Mpzl3 −/− mice developed sebaceous hypertrophy; *Mpzl3* and *rc* are allelic

To better understand *Mpzl3* function *in vivo*, we generated *Mpzl3* knockout mice. Exons 2~4, which encode the Ig domain and the transmembrane domain of MPZL3, were deleted and replaced by a *lacZ* reporter gene with an internal ribosome entry site (IRES) (Figure 1a). Loss of *Mpzl3* RNA and protein expression was confirmed with RT-PCR analysis and indirect immunofluorescent staining (Figure 1b, 1c).

Heterozygous (+/−) *Mpzl3* knockout mice were indistinguishable in gross appearance or skin histology from their wild type (+/+) littermates or *rc*/+ mice of the same age (Figure 1e, 1f, 1h, and below). Homozygous *Mpzl3* knockout (−/−) pups, however, started to show an unkempt hair coat and hair loss soon after birth (see below). Hematoxylin & eosin (H&E) staining of dorsal skin sections showed severe sebaceous gland (SG) hypertrophy in the *Mpzl3* −/− mice (Figure 1g), similar to that seen in the *rc/rc* mice (Figure 1i) as reported previously (Cao *et al.*, 2007; Hayashi *et al.*, 2004; Ruvinsky *et al.*, 2002). Additionally, the

rc/− mice, which are heterozygous for both mutant alleles, developed gross phenotype and sebaceous hypertrophy similar to the −/− and *rc/rc* mice (Figure 1g, 1i, 1j, 2a; Figure S1). These observations indicate that *Mpzl3* and *rc* are allelic; i.e., the *Mpzl3* missense mutation identified in the *rc* mice renders *Mpzl3* null, and directly causes the *rc* phenotype.

Oil Red O staining of dorsal skin sections confirmed SG hypertrophy in *Mpzl3* −/− mice (Figure 1k, 1l). Quantification detected a 5-fold increase in SG areas of the −/− mouse skin (P19, $p \ll 0.01$) (Figure 1m). PCNA staining of catagen (regression phase of the hair cycle) skin showed many more proliferating sebaceous precursors per gland in the −/− mouse skin than control (Figure 1n, 1o). These observations suggest that increased cell proliferation caused the sebaceous hypertrophy. *Mpzl3* −/− mouse skin also showed mild epidermal hyperplasia (Figure 1e, 1g). The pilary canal was also greatly enlarged, likely related to the SG hypertrophy (Figure 1g).

Gross phenotype and inflammatory skin phenotype in the *Mpzl3* −/− Mice

Phenotype analysis of *Mpzl3* knockout mice was carried out in C57BL/6 substrains with black or albino coat colors. Homozygous *Mpzl3* knockout (−/−) pups appeared normal at birth, but started to show an unkempt hair coat by 2 weeks after birth (P14) (Figure 2a). Albino −/− pups could actually be distinguished from their +/− and +/+ littermates even earlier by their “greasy” appearance (Figure 2a). By P18, as the dorsal skin enters the quiescent phase of the hair cycle (telogen), *Mpzl3* −/− mice displayed extensive, diffuse hair loss (Figure 2a). Hair grew back during the subsequent growth phase (anagen), but the hair coat remained unkempt and appeared greasy (Figure 2a). *Mpzl3* −/− mice developed recurrent alopecia in the dorsum (Figure 2a). Older −/− mice sometimes had patches of thin, short hair that lacked pigmentation, mimicking vellus hair in appearance (Figure 2a). *Mpzl3* −/− mice frequently had lower body weight than sex-matched +/+ or +/− littermates (Figure 2a and below).

The ratio among the offspring from *Mpzl3* +/− breeding followed Mendelian inheritance (N=156, κ^2=0.141. p=0.93), indicating there were no increased premature deaths of −/− embryos/pups compared with +/+ or +/− genotypes. *Mpzl3* −/− mice also lived a normal life expectancy.

In young *Mpzl3* −/− mice, in addition to the unkempt hair coat and alopecia, skin areas with less hair or areas prone to grooming and scratching (ears, muzzle, periorbital areas, upper chest, etc.) often appeared red, particularly in the albino mice (Figure 2b–2e). In juvenile −/− mice, dilated blood vessels were prominent in their ears (Figure 2b), and the muzzle skin appeared red and thickened (Figure 2c). By 4 months of age, −/− mice had developed alopecia and inflammatory lesions in these areas and the upper chest and anticubital areas (Figure 2d, 2e). Ear thickness was significantly greater in −/− mice compared with +/− littermates (0.19±0.029mm versus 0.23±0.027mm, mean±standard deviation, N=30 each, 1~8 months old, paired *t*-test, $p \ll 0.01$) (Figure 2h). Histological analysis revealed epidermal hyperplasia, hypergranulosis, hyperkeratosis and parakeratosis in the inflammatory skin lesions (Figure 2i–2l, Figure S2). There was increased dermal thickness with an inflammatory infiltrate consisting of neutrophils, lymphocytes and monocytes in affected skin (Figure 2i–2l, Figure S2). *Mpzl3* −/− mice older than 6 months frequently

developed scaly pink eczematous lesions of the muzzle with periorbital swelling, hair loss and occasional ocular involvement (Figure 2f, 2g). These mice also had skin ulcerations on the upper chest in areas where there had been alopecia (Figure 2g). Histologic evaluation of ulcers showed a diffuse monocytic and lymphocytic dermal infiltrate (Figure 2n).

Early onset skin phenotypes in the *Mpzl3* −/− mice were not caused by immune defects

To determine whether the early onset skin abnormalities were the results of a defective immune system, we generated *Mpzl3* −/− or control bone marrow chimeras in bone marrow reconstitution experiments. Lymphocyte-depleted bone marrow from *Mpzl3* −/− or +/+ mice was transferred to neonatal C57BL/6 Rag −/− mice (Figure 3a), which could not produce mature T cells or B cells on their own. The various immune compartments and lymphocyte activation status were analyzed by flow cytometry 10 weeks later, after immune reconstitution. The different immunological compartments analyzed included B cells, T cells, dendritic cells, macrophages and granulocytes. Ten week after bone marrow transfer, a functional immune system was reconstituted in both *Mpzl3* −/− and +/+ bone marrow recipients, and no significant differences were detected between the *Mplz3* −/− and control bone marrow chimeras (N=3 each) (Figure 3b). No skin abnormalities, in gross phenotype or histology, were detected in the mice that received *Mpzl3* −/− bone marrow, even at the end of 10 weeks (Figure 3c. 3d). Additionally, the spleen and inguinal lymph nodes (the skin-draining lymph nodes) of 7- and 10-day old *Mpzl3* −/− and +/− littermates (N=2 each) were also analyzed and no major differences were found in the different immunological compartments (data not shown). These results suggest that the early-onset skin abnormalities in the *Mplz3* −/− mice were not the results of defects in the immune system.

Hair loss and *Mpzl3* promoter activity during the hair cycle

To understand the cause of hair loss, we examined hair shafts removed by gentle pulling (P18). Many from the *Mpzl3* −/− mice showed breakage and lacked the club hair (Figure 4a, 4b), suggesting that the hair shafts may be brittle. Close examination of −/− mouse skin detected scales (Figure 4c, 4d) that resembled those observed in seborrheic dermatitis. To determine whether there were defects in hair shaft anchoring, we examined the expression of desmogleins (Dsg) in hair follicles (HFs). Dsg1/2 expression was detected abundantly in the −/− anagen HFs (Figure 4f), and Dsg3 in the −/− telogen HFs (Figure 4g). It remains to be determined what caused the severe hair loss during the first telogen.

We next determined *Mpzl3* promoter activity during the hair cycle by analyzing expression of the (knocked in) *lacZ* reporter gene (β-Gal) driven by the endogenous *Mpzl3* promoter. In newborn skin, β-Gal was detected in the suprabasal keratinocytes of the epidermis and elongating HFs (Figure 4h). As HF/SG morphogenesis progresses, at P10, β-Gal was detected in the epidermis, SG (Figure 4i), and the companion layer and the inner root sheath, but not the outer root sheath, of the HF (Figure 4j). There was only residual β-Gal in catagen/telogen HFs (Figure 4k). During the next anagen, at P25, β-Gal was detected in the newly formed inner root sheath/companion layer (Figure 4l). The observation that hair loss occurred during catagen/telogen, when *Mpzl3* promoter was of low activity, suggests that loss of *Mpzl3* function may have caused defects in structures formed during anagen.

Sebaceous gland hypertrophy and reduced dermal adipose tissue in the *Mpzl3 −/−* mice

Despite abundant *Mpzl3* expression in the newborn skin (Figure 1c), the dorsal skin of newborn *Mpzl3* −/− pups showed normal histology (Figure 5a, 5b). Additionally, expression of keratinocyte differentiation markers, such as keratin 14, keratin 10, loricrin and filaggrin, was comparable between −/− and +/+ dorsal skin in young mice (Figure S3).

To investigate the development of sebaceous hypertrophy, we carried out histological analysis of *Mpzl3* −/− and control littermate (+/+ or +/−) skin during postnatal hair follicle (HF) morphogenesis and the first hair cycle (Figure 5a–5n). No significant shifts in the morphogenesis or progression of the hair cycle were detected. However, by P10 at the latest, sebaceous hypertrophy had already become apparent in the −/− skin, and persisted thereafter (Figure 5e–5r), regardless of the phase of the hair cycle. Additionally, the dermal layer appeared thicker in the −/− skin than control (Figure 5). Furthermore, diffuse orthokeratotic hyperkeratotis was observed in −/− skin (Figure 5h, 5j, 5l, 5r). We also observed occasional foci of acanthosis (Figure 5r). Increased SG size and sebum production may be responsible for the greasy hair appearance (Figure 2a) and scales on the skin surface and hair shaft (Figure 5d) in the −/− mice.

Besides sebaceous hypertrophy, another striking feature of the *Mpzl3* −/− skin, especially in older mice, is the remarkably reduced thickness of the dermal adipose tissue (above the panniculus carnosus) (Figure 5o–5r). Of note, the dermal adipocytes in the *Mpzl3* −/− skin were of greatly reduced size (Figure 5p, 5r).

Reduced body weight and adiposity in the *Mpzl3 −/−* mice

We noticed that *Mpzl3* −/− mice frequently had lower body weight than sex-matched +/+ or +/− littermates (Figure 2a), and the dermal adipose tissue was much thinner in older −/− mice than controls (Figure 5o–5r). When we compared the growth curve of −/− mice and sex-matched +/− littermates (male N=5 each, female N=6 each) over a 14-week period, we detected a 16% reduction in the body weight of male −/− mice at 23 weeks, and a 23% reduction in female −/− mice (Figure 6a). *Mpzl3* −/− mice 6 months and older on average weighed only 70% of their sex-matched +/− or +/+ littermates (Figure S4). In addition to reduced cutaneous adipose tissue (Figure 5o–5r), −/− mice showed greatly reduced dorsal white adipose tissue (Figure 6b) and perigonadal white adipose tissue (Figure 6c). Similar observations were made in the *rc*/*rc* mice. In fact, the percentage total body fat was reduced by half in the *rc*/*rc* mice compared with sex-matched +/+ littermates (N=7 each, paired t-test, $p \ll 0.01$) (Figure 6d), even though their lean body mass was comparable (p=0.88) (Figure 6e). Oil Red O staining showed significantly reduced amount of lipids and lipid droplet size in the liver of fasting *rc*/*rc* mice (Figure 6f, 6g), suggesting that the absence of MPZL3 function resulted in either suppression of hepatic lipid accumulation or increased fat burning.

We also observed a 9% reduction in total bone mineral density (BMD) in the *rc/rc* mice (Figure 6h), as well as reduced BMD in the femur (data not shown). Of note, older *rc/rc* mice and *Mpzl3* −/− mice frequently developed kyphosis (Figure 6i, 6j). In our previous

study, we have documented loss of calcium in the femur and increased serum calcium level in the *rc/rc* mice (Hayashi *et al.*, 2004).

DISCUSSION

In this study, we showed that disruption of *Mpzl3* function caused severe cutaneous and extracutaneous abnormalities in mice. In the *Mpzl3* −/− mouse skin, we observed alopecia and sebaceous hypertrophy, epidermal hyperplasia and increased dermal thickness. *Mpzl3* −/− mice developed early onset, persistent inflammatory lesions, and we have shown that the early onset skin abnormalities were not caused by immune deficiencies. Another striking feature of the *Mpzl3* −/− mice is their greatly reduced adipose depots.

In a previous study, we detected a G→A missense mutation (consequently Arg100→Gln substitution) in the *Mpzl3* gene in the rough coat (*rc*) mice (Cao *et al.*, 2007). While both *rc*/+ and *Mpzl3* +/− mice were phenotypically and histologically normal, the *Mpzl3* −/− mice as well as mice heterozygous for both the knockout allele and the *rc* allele (*rc*/−) recapitulated abnormalities we previously described in the *rc*/*rc* mice (Figure 1, Figure S1) (Cao *et al.*, 2007; Hayashi *et al.*, 2004). These results provided unambiguous experimental evidence that *rc* and *Mpzl3* are allelic; that the G→A missense mutation in the *rc* mice (Cao *et al.*, 2007) renders *Mpzl3* null, and is the direct cause of the *rc* phenotype. Arg100 lies in the recognition loop of the Ig-like domain known for roles in antigen binding, cell–cell recognition and cell adhesion (Teichmann and Chothia, 2000; Vogel *et al.*, 2003), and is conserved in all vertebrate species sequenced to date (fish, amphibian, reptiles, birds, other mammals) (Racz *et al.*, 2009). Our results highlighted the functional significance of this residue for MPZL3 and possibly other Ig proteins. Since it is located in the extracellular region of a small single-span transmembrane protein (237 amino acids in mice and 235 amino acids in humans prior to cleavage of signal peptide), it may be possible to block MPZL3 function in potential therapeutics targeted at this residue or its vicinity.

Based on the knocked-in *lacZ* reporter gene expression during the hair cycle (Figure 4h–4l), *Mpzl3* promoter was already active at birth, had robust activity in the SG, the interfollicular epidermis, and the companion layer and the inner root sheath, but not the outer root sheath, of the HF. It is curious that hair loss did not occur when *Mpzl3* promoter was most active, during anagen, but occurred during catagen/telogen, when *Mpzl3* promoter was of low activity. It is possible that the MPZL3 protein contributed to structures formed during anagen that play a role in anchoring the hair shaft during telogen. Additionally, dilated pilary canal and hair shaft defects may also contribute to the alopecic phenotype. Detailed expression analysis of proteins involved in hair shaft formation and anchoring will lead to a better understanding of the underlying mechanism of hair loss (Kiso *et al.*, 2009; Koch *et al.*, 1998; Koch *et al.*, 1997; Tobin *et al.*, 2002).

It is not clear whether there is a direct cause-effect relationship between sebaceous hypertrophy and alopecia in *Mpzl3* −/− and *rc*/*rc* mice. It is interesting to note that while sebaceous hypertrophy became apparent in the *Mpzl3* −/− mice at least as early as P10, significant hair loss was not observed until the telogen phase a week later. Formation of the HF and SG, components of the pilosebaceous unit, is closely related, and involve both the

Wnt/β-catenin and hedgehog signaling, among others (Huelsken *et al.*, 2001; Kalderon, 2002; Kobielak *et al.*, 2003; Watt, 2004). It has been shown that reduced Wnt signaling and/or enhanced hedgehog signaling stimulates committed stem cell progenitors to differentiate toward the sebocyte lineage (Allen *et al.*, 2003; Han *et al.*, 2006; Horsley *et al.*, 2006; Merrill *et al.*, 2001; Niemann *et al.*, 2003; Takeda *et al.*, 2006). In the absence of MPZL3 function, no apparent defects were detected in HF morphogenesis (Figure 5a–5f). However, the SGs were clearly undergoing enhanced proliferation as sebaceous hypertrophy became apparent by P10 (Figure 5e, 5f). The failure to regrow hair in older mice lacking MPZL3 function could be a result of epithelial precursor cells stimulated for the sebaceous fate. Consistent with this hypothesis is our observation that older *Mpzl3* −/− and *rc*/*rc* mice showed patches of short, thin hair that mimicked vellus hair produced by miniaturized HFs (Figure 2a, Figure S5a). However, the HF stem cells/precursors likely remained as these mice were capable of regrowing long, thick, pigmented hair from the vellus-like patches, either spontaneously or upon anagen induction (Figure S5). Alternatively, the short vellus-like hair may be caused by shortened anagen, possibly related to the greatly reduced dermal adipose tissue. Recent studies have shown that intradermal adipocyte lineage cells are necessary and sufficient to drive HF stem cell activation (Festa *et al.*, 2011; Wojciechowicz *et al.*, 2013). Furthermore, a shortened anagen may also explain the lack of pigmentation in the newly formed hair shaft.

In addition to greatly reduced dermal adipose tissue, mice lacking MPZL3 function also showed significant reduction in the main adipose depots (Figure 6b, 6c), which contributed to a two-fold reduction in total body fat (Figure 6d). These results are consistent with a recent report by Statnick and colleagues in which they independently generated *Mpzl3* knockout mice deleting exon 3 (Czyzyk *et al.*, 2013). Their comprehensive study demonstrated that *Mpzl3* played a major role in body weight regulation, energy expenditure, glycemic control and hepatic triglyceride synthesis (Czyzyk *et al.*, 2013). In a large-scale knock-out project of secreted and transmembrane proteins, reduced body weight, fat mass and development of alopecia were also reported in *Mpzl3* knockout mice (Tang *et al.*, 2010). Adipocytes within the skin and subcutis are becoming recognized for more than just their roles in energy storage (Klein *et al.*, 2007; Schmidt and Horsley, 2012), as alopecia, hirsutism and hypertrichosis have been documented in cases with lipodystrophy (Agarwal and Garg, 2006; Fukumoto *et al.*, 2009; Savage *et al.*, 2007; Schmidt and Horsley, 2012) and obesity (Samara-Boustani *et al.*, 2012). It remains to be investigated whether alopecia in older *Mpzl3* −/− and *rc*/*rc* mice is directly related to the reduced dermal adipose tissue or a systemic effect of reduced adipose depots.

Results in this study suggest that *Mpzl3* is indispensible for skin functions and adiposity, and possibly bone mineral density. Skin disorders involving the SG such as acne vulgaris and inflammatory skin disorders account for millions of office visits each year (Mancini, 2008; Margolis *et al.*, 2012). Additionally, *Mpzl3* chromosomal location has been linked to control of body mass and energy expenditure (11q23.3) (Hanson *et al.*, 1998; Knowler *et al.*, 1978; Knowler *et al.*, 1991; Lindsay *et al.*, 2001; Norman *et al.*, 1998) and spine bone mineral density (11q14-q23) (Shen *et al.*, 2004). Given the high level of conservation between the

human and mouse *Mpzl3*, the *Mpzl3* −/− mice and *rc*/*rc* mice will serve as useful models to understand *Mpzl3* function in related human diseases.

MATERIALS AND METHODS

Generation of *Mpzl3* −/− mice and *rc*/− mice

All animal care and use procedures were approved by the University of Miami Institutional Animal Care and Use Committee (IACUC). Mice were maintained on a 12-hr light, 12-hr dark cycle at 22±1°C with controlled humidity, with access to water and rodent chow ad libitum. The *Mpzl3* targeting vector (with exons 2~4 deleted) was constructed at Knockout Mouse Project (KOMP, University of California, Davis, CA). Targeted JM8A3.N1 (*A/a; Tyr*$^{+/+}$) embryonic stem (ES) cells (CSD32805, *Mpzl3*$^{tm1(KOMP)Ucd}$) were verified at KOMP, and expanded and injected into C57BL/6-*Tyr*$^{c\text{-}Brd}$ (*a/a; Tyr*$^{c/c}$) mouse blastocysts at the Transgenic Animal Core Facility at the University of Miami Sylvester Comprehensive Cancer Center. Male chimeras were bred with albino C57BL/6 (*a/a; Tyr*$^{c/c}$) female mice to obtain G_1 offspring, which were crossed to obtain homozygous mutants. The colony was maintained in the C57BL/6N or mixed C57BL/6N x C57BL/6-*Tyr*$^{c\text{-}Brd}$ background, and mice with black or albino coats were used for analysis. Heterozygous rough coat (*rc*) mice (C57BL/6J-*Mpzl3*^{rc}/J) were purchased from the Jackson Laboratory (Bar Harbor, ME). Genotyping was achieved by PCR (Promega Corp., Madison, WI; Amresco, Solon, OH) of genomic DNA extracted from tail tip. Primer sequences are found in Table S1.

Histological analysis, immunohistochemistry, immunofluorescent staining and RT-PCR

Dorsal skin biopsies and other organs were collected from euthanized mice, fixed in 10% formalin, dehydrated and embedded in paraffin, before being cut into 5-μm sections and stained with hematoxylin and eosin (H&E). PCNA was detected by immunohistochemistry using a kit (Life Technologies Corp., Grand Island, NY). Beta-galactosidase activity was detected using a kit (Sigma-Aldrich, St. Louis, MO). Biopsies were also embedded in OCT, and 10-μm cryosections were processed and stained with Oil Red O for lipids. Images (25x, 100x, 200x and 400x) were captured using an Observer D1 microscope, and analyzed with AxioVision software (Carl Zeiss Microimaging Inc., Thornwood, NY).

Indirect immunofluorescent staining was carried out on cryosections using these primary antibodies: mouse anti-keratin 10 mAb, rabbit anti-keratin 14 pAb or rabbit anti-keratin 14 (FITC), rabbit anti-filaggrin pAb, rabbit anti-loricrin pAb (Covance, Princeton, NJ), rabbit anti-MPZL3 pAb (Cao *et al.*, 2007; Racz *et al.*, 2009), mouse anti-desmoglein 1/2 and 3 (Progen Biotechnik, Heidelberg, Germany) (kind gift of Dr. Lisa R. Plano, University of Miami), and goat anti-mouse IgG or goat anti-rabbit IgG (Alexa fluor 488) (Life Technologies Corp., Grand Island, NY) or goat anti-rabbit IgG (TRITC) (Sigma-Aldrich, St. Louis, MO). Sections were sometimes counterstained with Hoechst 33258 (AnaSpec, Fremont, CA).

Total RNA was extracted from mouse dorsal skin using TRIzol (Life Technologies Corp.) and RNeasy mini kit (Qiagen Inc., Valencia, CA). PCR (Promega Corp.) was carried out

after reverse transcription using a kit (Life Technologies Corp.). Primer sequences are found in Table S1.

Bone marrow reconstitution and analysis

Bone marrow was flushed out of femurs and tibias of *Mpzl3* −/− or +/+ littermates (6 weeks old). The bone marrow was labeled using biotinylated antibodies against CD3, CD4, CD8 and B220 (eBioscience, San Diego, CA). Streptavidin-labeled microbeads were then used to magnetically deplete the biotinylated lymphocytes using autoMACS (Milteyni Biotec, Inc., Auburn, CA). 3×10^6 bone marrow cells after depletion were injected intraperitoneally into 2-day old B6 Rag −/− mice (The Jackson Laboratory, Bar Harbor, ME). After 10 weeks, the inguinal lymph nodes and spleens of these mice were analyzed by flow cytometry, and skin analyzed by histology. For flow cytometry, 3×10^6 cells were blocked using a cocktail of anti-CD16/32 (2.4G2) and normal mouse sera (Jackson ImmunoResearch, West Grove, PA) before being stained with fluorescently labeled antibodies to determine their phenotype and activation status. The following antibody conjugates were used: CD11b PE-TR (Life Technologies Corp.), CD4 V500 (Becton Dickinson, San Jose, CA), CD11c FITC, Gr-1 PECy7, CD3 Alexa Fluor 700, CD8 efluor605, B220 PerCpCy5.5, CD44 efluor450, CD62L APC, CD69 PE (eBioscience). Cells were then washed and re-suspended in 2% FBS in PBS for analysis with flow cytometers (LSR-II and Fortessa, Becton Dickinson).

Measurements in live mice: weight, ear thickness and whole body composition

Male and female, sex-matched *Mpzl3* +/− and −/− littermates were weighed weekly from 9 weeks to 23 weeks. Ear thickness was measured in *Mpzl3* +/− and −/− littermates using a caliper rule (Thermo Fisher Scientific Inc., Waltham, MA). Lean mass, fat mass and bone mineral density in *rc/rc* and +/+ littermates were measured by dual-energy X-ray absorptiometry (DEXA, Lunar PIXI) (Lunar, Madison, WI). Mice were anesthetized with intraperitoneal injections of ketamine/xylazine (80mg/kg and 10mg/kg) (Sigma-Aldrich, St. Louis, MO) and scanned in the prone position.

Supplementary Material

Refer to Web version on PubMed Central for supplementary material.

Acknowledgments

This work was supported by NIH/NIAMS grants K01AR050487 and R03AR059907 (T.C.W.), a Dermatology Foundation Research Grant (T.C.W.), and the Dermatology Gift Fund, University of Miami (T.C.W.). The *Mpzl3* knockout mouse strain generated for this research project was created from embryonic stem cell lines obtained from the NCRR-NIH supported KOMP Repository (www.komp.org) at the University of California Davis. Mouse embryonic stem cell expansion and blastocyst injections were carried out at the University of Miami Sylvester Comprehensive Cancer Center Transgenic Animal Core Facility (Director: Peter Sobieszczuk, Ph.D.). The mouse anti-desmoglein 1/2 and 3 antibodies (Progen Biotechnik, Heidelberg, Germany) were kindly provided by Dr. Lisa R. Plano, University of Miami. T.C.W. is very grateful for mentoring from Dr. Katalin Csiszar (University of Hawaii at Manoa). She would also like to thank Anika J.W. and Athula H.W. The authors would like to thank Dr. Lawrence A. Schachner for his support, and Drs. Carmen I. Perez, Juana Alonso, Luis Rodriguez-Menocal, and Assuan Lens and Irene A. Tabas for technical assistance.

Abbreviations

BMD	bone mineral density
Dsg	desmoglein
HF	hair follicle
H&E	hematoxylin and eosin
Ig	immunoglobulin
IRES	internal ribosome entry site
Mpzl3	Myelin protein zero-like 3
rc	rough coat
SG	sebaceous gland

References

1. Agarwal AK, Garg A. Genetic disorders of adipose tissue development, differentiation, and death. Annu Rev Genomics Hum Genet. 2006; 7:175–199. [PubMed: 16722806]
2. Allen M, Grachtchouk M, Sheng H, Grachtchouk V, Wang A, Wei L, et al. Hedgehog signaling regulates sebaceous gland development. Am J Pathol. 2003; 163:2173–2178. [PubMed: 14633591]
3. Cao T, Racz P, Szauter KM, Groma G, Nakamatsu GY, Fogelgren B, et al. Mutation in Mpzl3, a novel [corrected] gene encoding a predicted [corrected] adhesion protein, in the rough coat (rc) mice with severe skin and hair abnormalities. J Invest Dermatol. 2007; 127:1375–1386. [PubMed: 17273165]
4. Czyzyk TA, Andrews JL, Coskun T, Wade MR, Hawkins ED, Lockwood JF, et al. Genetic ablation of myelin protein zero-like 3 in mice increases energy expenditure, improves glycemic control, and reduces hepatic lipid synthesis. Am J Physiol Endocrinol Metab. 2013; 305:E282–292. [PubMed: 23715724]
5. Dickie MM. Rough coat. Mouse News Letter. 1966; 34:30.
6. Eicher EM, Fox S, Reynolds S. Rough coat on Chromosome 9. Mouse News Letter. 1977; 56:42.
7. Festa E, Fretz J, Berry R, Schmidt B, Rodeheffer M, Horowitz M, et al. Adipocyte lineage cells contribute to the skin stem cell niche to drive hair cycling. Cell. 2011; 146:761–771. [PubMed: 21884937]
8. Fukumoto D, Kubo Y, Saito M, Arase S. Centrifugal lipodystrophy of the scalp presenting with an arch-form alopecia: a 10-year follow-up observation. J Dermatol. 2009; 36:499–503. [PubMed: 19712277]
9. Han G, Li AG, Liang YY, Owens P, He W, Lu S, et al. Smad7-induced beta-catenin degradation alters epidermal appendage development. Dev Cell. 2006; 11:301–312. [PubMed: 16950122]
10. Hanson RL, Ehm MG, Pettitt DJ, Prochazka M, Thompson DB, Timberlake D, et al. An autosomal genomic scan for loci linked to type II diabetes mellitus and body-mass index in Pima Indians. Am J Hum Genet. 1998; 63:1130–1138. [PubMed: 9758619]
11. Hayashi K, Cao T, Passmore H, Jourdan-Le Saux C, Fogelgren B, Khan S, et al. Progressive hair loss and myocardial degeneration in rough coat mice: reduced lysyl oxidase-like (LOXL) in the skin and heart. J Invest Dermatol. 2004; 123:864–871. [PubMed: 15482472]
12. Horsley V, O'Carroll D, Tooze R, Ohinata Y, Saitou M, Obukhanych T, et al. Blimp1 defines a progenitor population that governs cellular input to the sebaceous gland. Cell. 2006; 126:597–609. [PubMed: 16901790]
13. Huelsken J, Vogel R, Erdmann B, Cotsarelis G, Birchmeier W. beta-Catenin controls hair follicle morphogenesis and stem cell differentiation in the skin. Cell. 2001; 105:533–545. [PubMed: 11371349]

14. Kalderon D. Similarities between the Hedgehog and Wnt signaling pathways. Trends Cell Biol. 2002; 12:523–531. [PubMed: 12446114]
15. Kiso M, Tanaka S, Saba R, Matsuda S, Shimizu A, Ohyama M, et al. The disruption of Sox21-mediated hair shaft cuticle differentiation causes cyclic alopecia in mice. Proc Natl Acad Sci U S A. 2009; 106:9292–9297. [PubMed: 19470461]
16. Klein J, Permana PA, Owecki M, Chaldakov GN, Bohm M, Hausman G, et al. What are subcutaneous adipocytes really good for? Exp Dermatol. 2007; 16:45–70. [PubMed: 17181636]
17. Knowler WC, Bennett PH, Hamman RF, Miller M. Diabetes incidence and prevalence in Pima Indians: a 19-fold greater incidence than in Rochester, Minnesota. Am J Epidemiol. 1978; 108:497–505. [PubMed: 736028]
18. Knowler WC, Pettitt DJ, Saad MF, Charles MA, Nelson RG, Howard BV, et al. Obesity in the Pima Indians: its magnitude and relationship with diabetes. Am J Clin Nutr. 1991; 53:1543S–1551S. [PubMed: 2031485]
19. Kobielak K, Pasolli HA, Alonso L, Polak L, Fuchs E. Defining BMP functions in the hair follicle by conditional ablation of BMP receptor IA. J Cell Biol. 2003; 163:609–623. [PubMed: 14610062]
20. Koch PJ, Mahoney MG, Cotsarelis G, Rothenberger K, Lavker RM, Stanley JR. Desmoglein 3 anchors telogen hair in the follicle. J Cell Sci. 1998; 111 (Pt 17):2529–2537. [PubMed: 9701552]
21. Koch PJ, Mahoney MG, Ishikawa H, Pulkkinen L, Uitto J, Shultz L, et al. Targeted disruption of the pemphigus vulgaris antigen (desmoglein 3) gene in mice causes loss of keratinocyte cell adhesion with a phenotype similar to pemphigus vulgaris. J Cell Biol. 1997; 137:1091–1102. [PubMed: 9166409]
22. Lindsay RS, Kobes S, Knowler WC, Bennett PH, Hanson RL. Genome-wide linkage analysis assessing parent-of-origin effects in the inheritance of type 2 diabetes and BMI in Pima Indians. Diabetes. 2001; 50:2850–2857. [PubMed: 11723070]
23. Mancini AJ. Incidence, prevalence, and pathophysiology of acne. Adv Stud Med. 2008; 8:100–105.
24. Margolis DJ, Apter AJ, Gupta J, Hoffstad O, Papadopoulos M, Campbell LE, et al. The persistence of atopic dermatitis and filaggrin (FLG) mutations in a US longitudinal cohort. J Allergy Clin Immunol. 2012; 130:912–917. [PubMed: 22951058]
25. Merrill BJ, Gat U, DasGupta R, Fuchs E. Tcf3 and Lef1 regulate lineage differentiation of multipotent stem cells in skin. Genes Dev. 2001; 15:1688–1705. [PubMed: 11445543]
26. Niemann C, Unden AB, Lyle S, Zouboulis ChC, Toftgard R, Watt FM. Indian hedgehog and beta-catenin signaling: role in the sebaceous lineage of normal and neoplastic mammalian epidermis. Proc Natl Acad Sci U S A. 2003; 100(Suppl 1):11873–11880. [PubMed: 12917489]
27. Norman RA, Tataranni PA, Pratley R, Thompson DB, Hanson RL, Prochazka M, et al. Autosomal genomic scan for loci linked to obesity and energy metabolism in Pima Indians. Am J Hum Genet. 1998; 62:659–668. [PubMed: 9497255]
28. Racz P, Mink M, Ordas A, Cao T, Szalma S, Szauter KM, et al. The human orthologue of murine Mpzl3 with predicted adhesive and immune functions is a potential candidate gene for immune-related hereditary hair loss. Exp Dermatol. 2009; 18:261–263. [PubMed: 19054061]
29. Ramani SR, Tom I, Lewin-Koh N, Wranik B, Depalatis L, Zhang J, et al. A secreted protein microarray platform for extracellular protein interaction discovery. Anal Biochem. 2012; 420:127–138. [PubMed: 21982860]
30. Ruvinsky I, Chertkov O, Borue XV, Agulnik SI, Gibson-Brown JJ, Lyle SR, et al. Genetics analysis of mouse mutations Abnormal feet and tail and rough coat, which cause developmental abnormalities and alopecia. Mamm Genome. 2002; 13:675–679. [PubMed: 12514744]
31. Samara-Boustani D, Colmenares A, Elie C, Dabbas M, Beltrand J, Caron V, et al. High prevalence of hirsutism and menstrual disorders in obese adolescent girls and adolescent girls with type 1 diabetes mellitus despite different hormonal profiles. Eur J Endocrinol. 2012; 166:307–316. [PubMed: 22127492]
32. Savage DB, Semple RK, Chatterjee VK, Wales JK, Ross RJ, O'Rahilly S. A clinical approach to severe insulin resistance. Endocr Dev. 2007; 11:122–132. [PubMed: 17986832]
33. Schmidt B, Horsley V. Unravelling hair follicle-adipocyte communication. Exp Dermatol. 2012; 21:827–830. [PubMed: 23163647]

34. Shen H, Zhang YY, Long JR, Xu FH, Liu YZ, Xiao P, et al. A genome-wide linkage scan for bone mineral density in an extended sample: evidence for linkage on 11q23 and Xq27. J Med Genet. 2004; 41:743–751. [PubMed: 15466007]

35. Takeda H, Lyle S, Lazar AJ, Zouboulis CC, Smyth I, Watt FM. Human sebaceous tumors harbor inactivating mutations in LEF1. Nat Med. 2006; 12:395–397. [PubMed: 16565724]

36. Tang T, Li L, Tang J, Li Y, Lin WY, Martin F, et al. A mouse knockout library for secreted and transmembrane proteins. Nat Biotechnol. 2010; 28:749–755. [PubMed: 20562862]

37. Teichmann SA, Chothia C. Immunoglobulin superfamily proteins in Caenorhabditis elegans. J Mol Biol. 2000; 296:1367–1383. [PubMed: 10698639]

38. Tobin DJ, Foitzik K, Reinheckel T, Mecklenburg L, Botchkarev VA, Peters C, et al. The lysosomal protease cathepsin L is an important regulator of keratinocyte and melanocyte differentiation during hair follicle morphogenesis and cycling. Am J Pathol. 2002; 160:1807–1821. [PubMed: 12000732]

39. Vogel C, Teichmann SA, Chothia C. The immunoglobulin superfamily in Drosophila melanogaster and Caenorhabditis elegans and the evolution of complexity. Development. 2003; 130:6317–6328. [PubMed: 14623821]

40. Watt FM. Unexpected Hedgehog-Wnt interactions in epithelial differentiation. Trends Mol Med. 2004; 10:577–580. [PubMed: 15567325]

41. Wojciechowicz K, Gledhill K, Ambler CA, Manning CB, Jahoda CA. Development of the mouse dermal adipose layer occurs independently of subcutaneous adipose tissue and is marked by restricted early expression of FABP4. PLoS One. 2013; 8:e59811. [PubMed: 23555789]

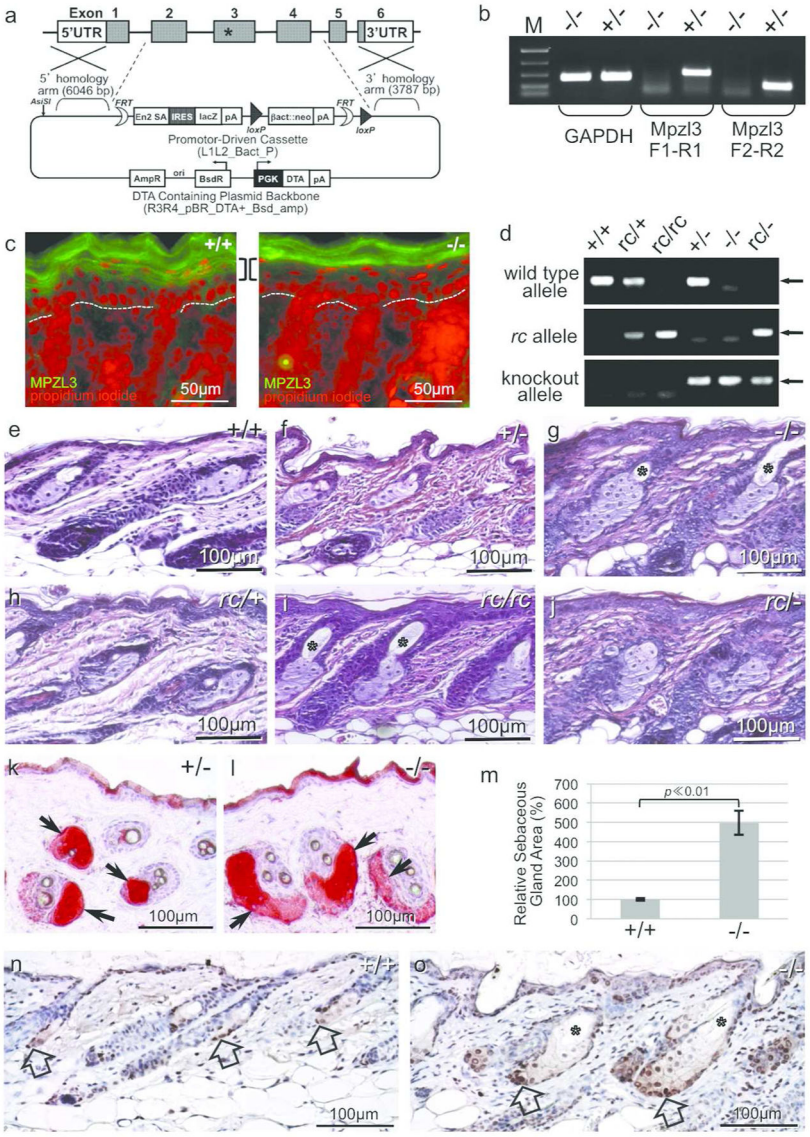

Figure 1. *Mpzl3* knockout (−/−) mice and *rc*/− mice developed sebaceous gland hypertrophy as seen in the *rc*/*rc* mice

(a) Targeting vector to generate *Mpzl3* knockout mice. Exons 2 to 4 were deleted and replaced with a *lacZ* reporter gene with IRES. The asterisk in exon 3 denotes the point mutation in the *rc* mice. (b) RT-PCR analysis confirming loss of *Mpzl3* RNA expression in *Mpzl3* knockout mouse skin. (c) Indirect immunofluorescent staining confirming loss of MPZL3 protein expression in suprabasal keratinocytes (brackets) in *Mpzl3* knockout mouse skin (P2). Dotted lines denote the location of the basement membrane. Positive staining in the stratum corneum is an artifact. Scale bars = 50 μm. (d) PCR genotyping of the various *Mpzl3* alleles. (e–j) Hematoxylin and eosin (H&E) staining of dorsal skin sections from sex-matched mice (P24). Sebaceous gland hypertrophy was observed in the skin of *Mpzl3* −/− mice (g), *rc*/*rc* mice (i) and mice heterozygous for both the *rc* allele and the *Mpzl3* knockout allele (*rc*/−) (j), but not in *Mpzl3* +/− (f), *rc*/+ (h) or wild type (e) mice, indicating that *Mpzl3* and *rc* are allelic. Scale bars = 100 μm. (k, l) Oil Red O staining of lipids in the sebaceous

glands (arrows). Mice were 5 months old. Scale bars = 100 μm. (m) Quantitative analysis of sebaceous gland area in skin sections of *Mpzl3* −/− and +/+ littermates (P19). Bars=standard error of mean. (n, o) Hyperproliferation of sebocyte precursors in the *Mpzl3* −/− skin by PCNA staining (brown, counterstained with hematoxylin). Block arrows point to the many proliferating cells in the *Mpzl3* −/− sebaceous glands (o) compared with +/+ skin (n) (P19). Asterisk: enlarged pilary canal in the *Mpzl3* −/− skin (g, i, o). Scale bars = 100 μm.

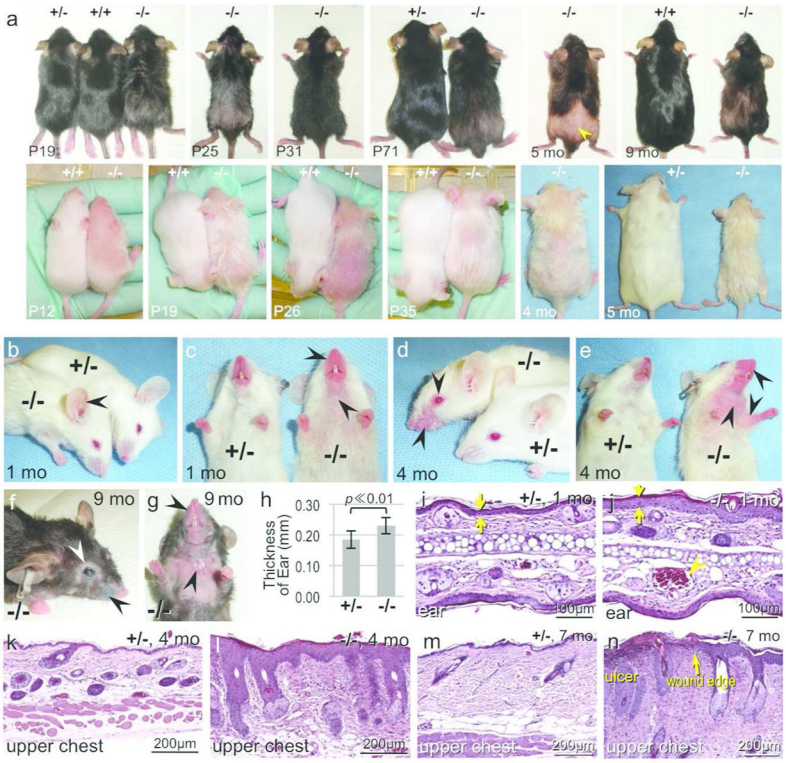

Figure 2. Gross phenotype and inflammatory skin phenotype of the *Mpzl3* −/− mice

(a) Gross phenotype of *Mpzl3* +/+, +/− and −/− littermates at the ages indicated. Mice shown were in the C57BL/6 strain with black or albino coat colors. *Mpzl3* −/− mice developed recurrent alopecia, and patches of regrown hair had vellus-like appearance (arrowhead). *Mpzl3* −/− mice frequently had lower body weight than control littermates (the pairs at 5 and 9 months of age). (b–g) Development of inflammatory skin lesions in *Mpzl3* −/− mice but not control littermates. Dilated blood vessels in the ear (b); redness of the muzzle, upper chest and anticubital areas (c, e); red, scaly eczematous lesions on the muzzle (c, e); periorbital swelling and hair loss (d, f), loss of most vibrissae (e–g), inflammatory lesions of the eye (f), and persistent ulceration in the upper chest (g). (h) The thickness of the ear in *Mpzl3* +/− and −/− littermates. Bar=standard deviation, N=30 each, 1–8 months old. (i–n) H&E staining of lesional skin from *Mpzl3* −/− mice (j, l, n) compared with location-matched skin from +/− littermates (i, k, m). *Mpzl3* −/− skin showed epidermal hyperplasia (opposing arrows), hypergranulosis, hyperkeratosis and lymphocyte/monocyte infiltration, increased dermal thickness, dilated blood vessel in the ear (arrowhead) (j), sebaceous hypertrophy (l, n), ulcer in the upper chest area (n), with epidermal hyperplasia and parakeratosis in the wound edge (arrow) and diffuse leukocyte infiltration in the dermis (n). Scale bars = 100 μm (i, j), scale bars = 200 μm (k–n).

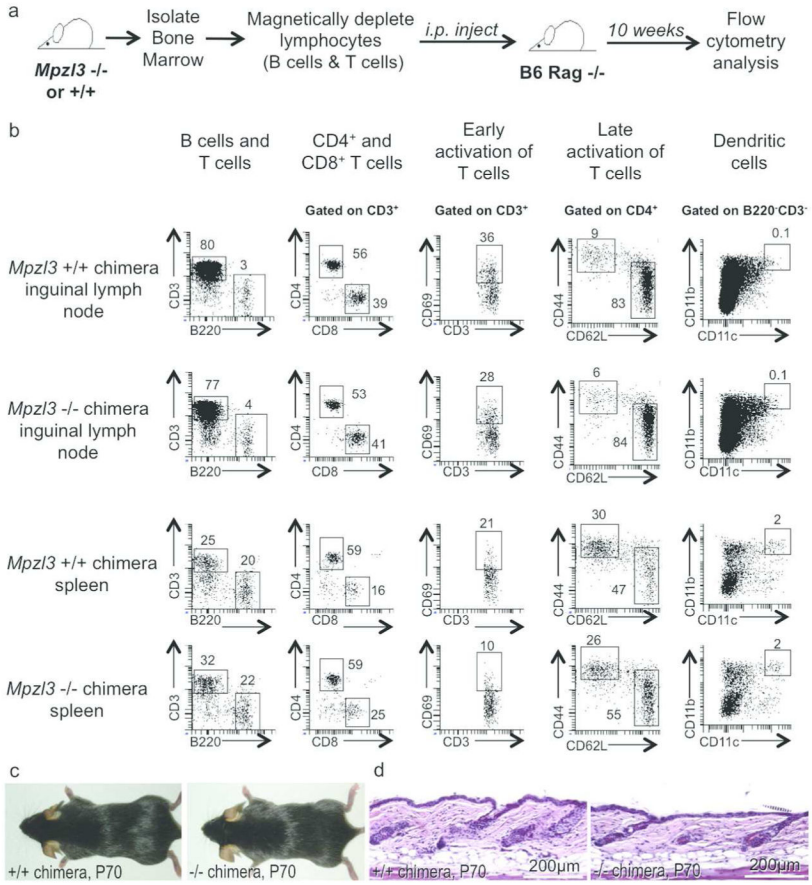

Figure 3. Flow cytometry of reconstituted immune populations in bone marrow chimeras between *Mpzl3* −/− or +/+ mice and immunodeficient Rag knockout mice

(a) Schematic diagram of the procedure. (b) Representative flow cytometry plots of one pair of reconstituted mice (N=3 each), showing immune cell phenotypes in inguinal lymph nodes (top two rows) that drain the skin, and in the spleen (bottom two rows) that drain the blood circulation. Different surface markers were used for flow cytometry analysis to study different immune populations as indicated. *Numbers in plots represent percentage of parent population.* (c, d) Gross phenotype (c) and dorsal skin histology (d) of the chimeras showed no apparent differences. Scale bars = 200 μm.

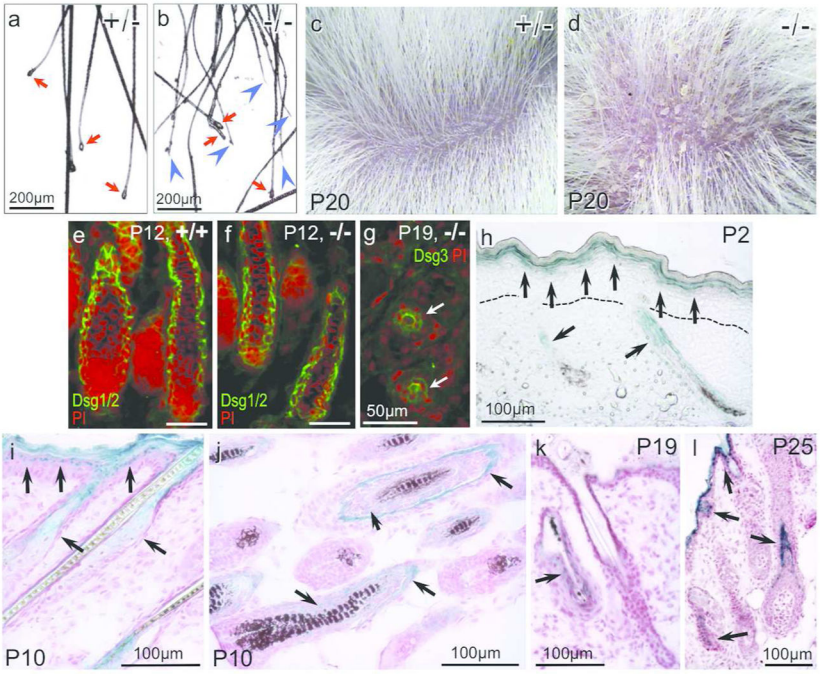

Figure 4. Hair loss in the *Mpzl3* −/− mice and detection of *Mpzl3* promoter activity during the first hair cycle

(a, b) Breakage of the hair shaft (blue arrowheads) from an *Mpzl3* −/− mouse (b), but not +/− littermate (a) (P18). Red arrows point to the club hair (a, b). Scale bars = 200 μm. (c, d) Scales were observed in *Mpzl3* −/− mouse skin (P20) (d), but not +/− littermate skin (c). (e–g) Expression of desmogleins (Dsg) in anagen (e, f) and telogen (g) hair follicles of +/+ (e) and *Mpzl3* −/− (f, g) skin. Scale bars = 50 μm. (h–l) *Mpzl3* promoter activity detected by reporter gene *lacZ* expression in *Mpzl3* −/− skin. *LacZ* expression (blue) was detected in the suprabasal layers of the epidermis (h, i, l), sebaceous gland (i), and the companion layer and the inner root sheath (arrows) but not the outer root sheath of the hair follicles (j, l) during anagen (h–j, l), and at low levels during catagen/telogen (k). Sections were counterstained with nuclear fast red (i–l). Dotted lines denote the location of the basement membrane (h). Scale bars = 100 μm.

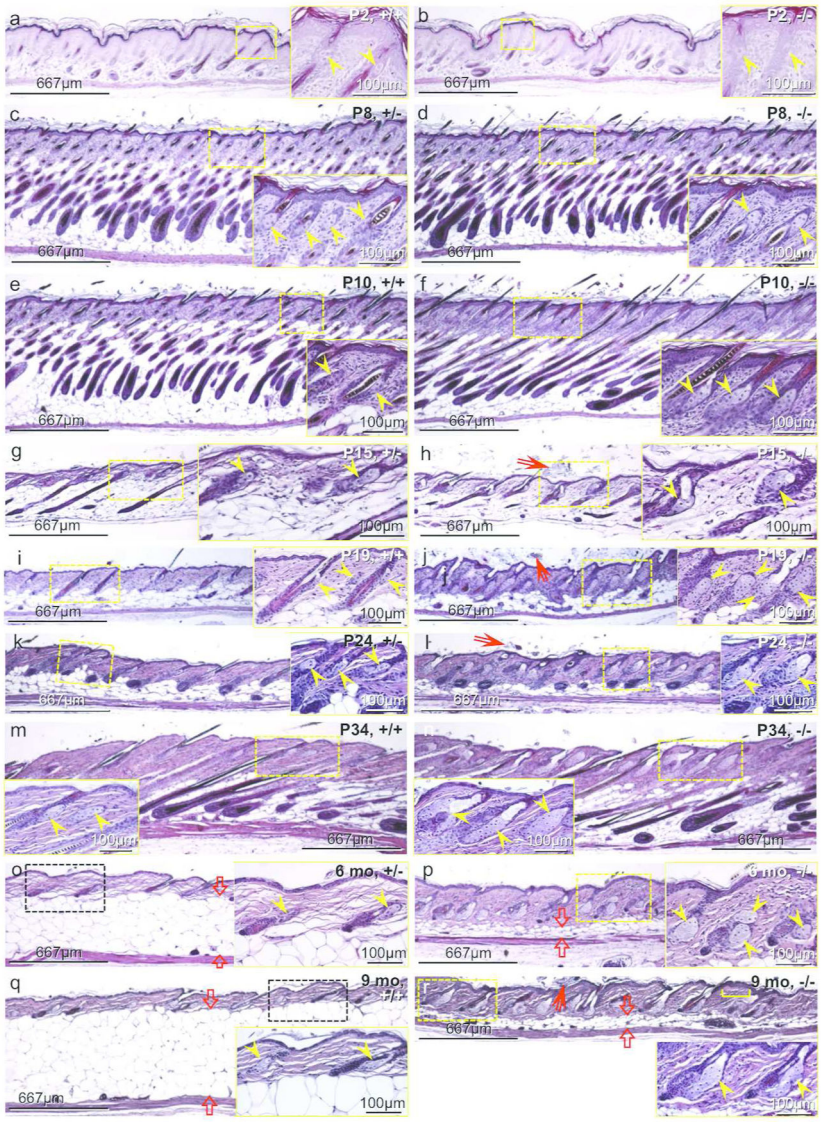

Figure 5. Development of sebaceous hypertrophy and greatly reduced dermal adipose tissue in the *Mpzl3* −/− mice

H&E staining of location-matched dorsal skin sections of *Mpzl3* −/− mice (b, d, f, h, j, l, n, p, r) and sex-matched control (+/+ or +/−) littermate (a, c, e, g, i, k, m, o, q). Paired images (including insets) in the same row are shown at the same magnification. Original magnification: 40x. Images were also captured at 200x (insets) to show details of the sebaceous glands. Yellow arrowheads: sebaceous glands; red arrows: orthokeratotic hyperkeratotis (h, j, l, r); yellow bracket: a focus of acanthosis (r); opposing red block arrows: thickness of the cutaneous adipose tissue (o–r). Scale bars = 667 μm (Scale bars = 100 μm in insets).

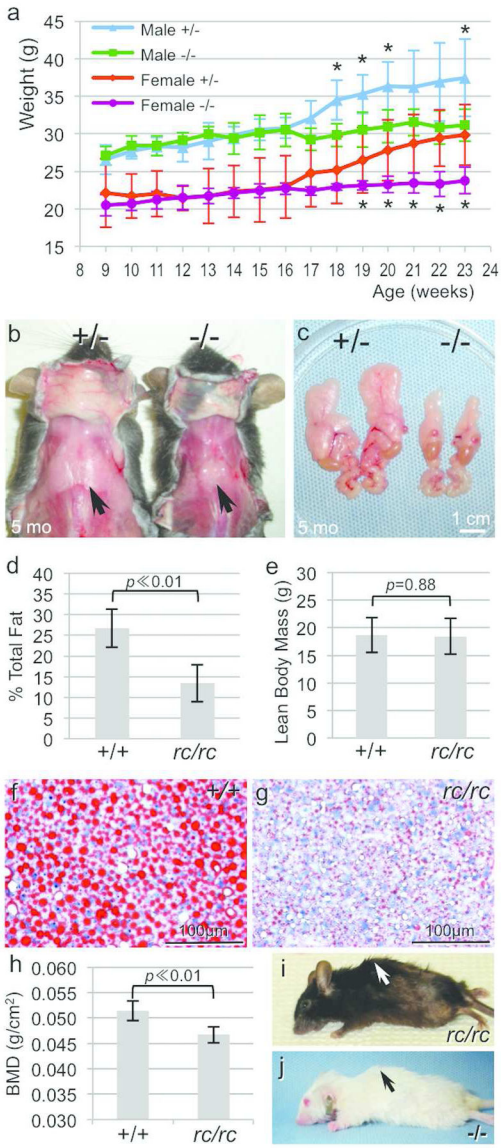

Figure 6. Reduced adiposity and bone mineral density in the *Mpzl3* −/− and *rc*/*rc* mice

(a) Growth curve of male and female *Mpzl3* −/− mice compared with sex-matched +/− littermates over 14 weeks. N=5 each for males, N=6 each for females. Bars = standard deviation, Asterisk (*): $p<0.05$. (b, c) Reduced dorsal (b) and epididymal (c) white adipose tissue in the *Mpzl3* −/− mice compared with sex-matched +/− littermates. Scale bar = 1 cm. (d, e) Significantly decreased total body fat (d), but not lean mass (e), in the *rc*/*rc* mice compared with sex-matched +/+ littermates. N=7 each. Bars = standard deviation, paired *t*-test. (f, g) Oil Red O staining showing reduced hepatic lipids in the liver of fasting +/+ (f) and *rc*/*rc* (g) littermates. Scale bars = 100 μm. (h) Total bone mineral density (BMD) in the *rc/rc* mice and their sex-matched +/+ littermates. N=7 each, bars = standard deviation, paired *t*-test. (i, j) Kyphosis in *rc/rc* (i) and *Mpzl3* −/− (j) mice.